High energy density of PLZST antiferroelectric ceramics

prepared by sol-gel method with low-cost dibutyltin oxide

Yu Dan ¹, Haojie Xu ¹, Yangyang Zhang ², Kailun Zou ¹, Qingfeng Zhang ^{1,*}, Yinmei Lu ¹, Gang Chang ¹, Qi Zhang ³, Yunbin He ^{1,*}

¹Hubei Collaborative Innovation Center for Advanced Organic Chemical Materials, Hubei Key Lab of Ferro

& Piezoelectric Materials and Devices, Ministry of Education Key Laboratory of Green Preparation and

Application for Functional Materials, School of Materials Science & Engineering, Hubei University, Wuhan

430062, China

²Henan Provincial Key Laboratory of Nanocomposites and Applications, Institute of Nanostructured

Functional Materials, Huanghe Science and Technology College, Zhengzhou 450006, China

³Department of Manufacturing and Materials, Cranfield University, Cranfield, Bedfordshire, MK43 0AL,

UK

Abstract

Lead lanthanum zirconate stannate titanate (PbLa(ZrSnTi)O₃) antiferroelectric (AFE) ceramics

are widely used in dielectric capacitors due to their superior energy-storage capacity. Generally,

these ceramics can be synthesized by solid-state reaction and sol-gel methods. Ceramics

prepared using the sol-gel method have a purer phase than those prepared using the solid-state

reaction method because the sol-gel method can avoid the segregation of Sn. However, because

the commonly used raw material tin acetate is very expensive, the preparation of

PbLa(ZrSnTi)O₃ AFE ceramics via the sol-gel method is not cost-effective, which prevents the

use of sol-gel method for manufacturing PbLa(ZrSnTi)O3 in a large scale. In this work,low-

cost dibutyltin oxide instead of expensive tin acetate is used to synthesize Pb_{0.97}La_{0.02}(Zr_{0.50}Sn_{0.45}Ti_{0.05})O₃ (PLZST) nanopowders, and single-phase powders with a perovskite structure and average grain size of 200 nm are obtained at a calcination temperature of 580 °C. In addition, dense PLZST AFE ceramics with a pure perovskite structure are obtained by sintering the PLZST nanopowders at temperatures as low as 1100 °C. The sintered PLZST ceramics exhibit a room-temperature recoverable energy-storage density as high as 1.93 J/cm³ with an efficiency of 75%, which varies only slightly in the temperature range of 20-120 °C. The high energy-storage density (>1.9 J/cm³) over a wide temperature range illustrates that the sol-gel-derived PLZST ceramics with low-cost dibutyltin oxide are quite promising for manufacturing pulse power capacitors.

1. INTRODUCTION

With the rapid development of power systems and modern electronic technology, an urgent need exists for high-performance energy-storage systems. Current energy-storage devices include batteries, fuel cells, electrochemical capacitors, and dielectric capacitors. Of these devices, dielectric capacitors offer the advantages of high power density, fast charge and discharge process ($<1~\mu s$), low cost, and high thermal stability. Therefore, they are widely used in hybrid electric vehicles, medical devices, mobile electronic devices, and electronic weapon systems. At present, the prevalent materials used for dielectric capacitors are antiferroelectrics (AFEs), ferroelectrics (FEs), and linear dielectrics. Compared with FE materials and linear dielectric materials, AFE materials have the advantages of high energy storage capacity and fast charge and discharge speed due to their near zero remnant polarization P_r and unique character of field-induced switching between AFE and FE phases. Thus, AFE materials have drawn an increasing attention in recent years towards capacitor applications.

Over the past few years, extensive research on AFE based energy-storage materials has focused on ceramics based on lead lanthanum zirconate stannate titanate (PbLa(ZrSnTi)O₃) because of their superior energy storage properties. ¹⁴⁻¹⁸ At present, two main techniques exist for preparing PbLa(ZrSnTi)O₃ ceramic powders: the traditional solid-state reaction technique and the liquid-state synthesis technique. ¹⁹⁻²¹ The traditional solid-state reaction technique has been more widely used, in which the PbLa(ZrSnTi)O₃ powders are manufactured through solid-state reaction at high temperatures and its advantages include simple processing and low cost. However, the high calcination temperature leads not only to high energy consumption, but also to the volatilization of Pb, which often generates an impurity phase. In addition, the segregation of Sn can easily occur when the Sn content in PbLa(ZrSnTi)O₃ is high. ²² Compared with the solid-state technique, the liquid-state synthesis technique offers advantages of controlled chemical composition, high chemical homogeneity, high purity, high activity, low

synthesis temperature, and small resulting powder particles.²³ Liquid-state synthesis technique mainly includes coprecipitation, ^{24,25} hydrothermal method, ²⁶ and sol-gel method.²⁷ Of these methods, the sol-gel method has been widely used to prepare PbLa(ZrSnTi)O₃ powders, ^{28,29} due to the requirement of only simple equipment. However, in previous reports regarding the synthesis of PbLa(ZrSnTi)O₃ powders via the sol-gel method, Sn element is usually supplied by tin acetate. Unfortunately, tin acetate is expensive (circa 88 \$ per gram), leading to a high production cost of the sol-gel synthesis method, and thus precluding a large-scale fabrication of PbLa(ZrSnTi)O₃ powders. In contrast, alternative Sn precursor, dibutyltin oxide, is much inexpensive with a price of about 0.4 \$ per gram. If dibutyltin oxide can really be used as the Sn precursor for the sol-gel synthesis of PbLa(ZrSnTi)O₃ powders, the production cost can be reduced substantially, and thus large-scale manufacturing of PbLa(ZrSnTi)O₃ AFE based capacitors becomes viable. However, the sol-gel synthesis of PbLa(ZrSnTi)O₃ powders with dibutyltin oxide has been scarcely documented in literature so far.

In the present work, we have attempted using theinexpensive dibutyltin oxide instead of tin acetate to synthesize high-Sn-content Pb_{0.97}La_{0.02}(Zr_{0.50}Sn_{0.45}Ti_{0.05})O₃ (PLZST) powders. Via this modified cost-effective sol-gel method, single-perovskite phase PLZST nanopowders are obtained, based on which dense ceramics are further fabricated at a low temperature of 1100 °C. More interestingly, the PLZST AFE ceramics prepared using these nanopowders show remarkably better energy-storage performance than those prepared with the traditional solid-state reaction method at a much higher sintering temperature.

2. EXPERIMENTAL PROCEDURE

We used the modified sol-gel method to synthesize Pb_{0.97}La_{0.02}(Zr_{0.50}Sn_{0.45} Ti_{0.05})O₃ AFE powders. Lead acetate trihydrate (Pb(CH₃COO)₂·3H₂O, 99.5%, Sinopharm), lanthanum acetate (La(CH₃COO)₃, 99.9%, Macklin), dibutyltin oxide ((H₉C₄)₂SnO, 98%, Macklin),

zirconium propoxide (Zr(OC₃H₇)₄, 70%, Aladdin) and titanium isopropoxide (Ti[OCH(CH₃)₂]₄, 95%, Aladdin) were used as the main raw materials. Lactic acid (C₃H₆O₃, 85%, Sinopharm) served as a chelating agent, deionized water (H₂O) served as stabilizer, and polyethylene glycol (HO(CH₂CH₂O)_nH, 99%, Macklin) (PEG) served as dispersing agent. Acetic acid (CH₃COOH, 99.9%, Sinopharm) was used as a solvent.

At first, lead acetate trihydrate (with 3% excess amount to compensate for Pb volatilization at high temperature), dibutyltin oxide, lanthanum acetate hydrate, and acetic acid were mixed in a predetermined ratio and the solution was stirred for 30 minutes at 90 °C. Once the mixed solution (precursor A) was cooled to room temperature, appropriate amounts of zirconium propoxide and titanium isopropoxide were added and the solution was stirred for 120 minutes. While mixing, deionized water (lead acetate : deionized water = 1M : 20M) was rapidly added to stabilize the solution. Meanwhile, 10 ml diethanolamine (C₄H₁₁NO₂, 99%, Macklin) was added to the solution to reduce the synthesis temperature of the PLZST powders. The exothermic decomposition of diethanolamine releases considerable energy, which promotes the crystallization of the perovskite phase at a relatively low temperature. Next, lactic acid (1 mL per 10 g of lead acetate) was dropped into the solution (precursor B) and slowly mixed for 30 minutes, and then 8 g of polyethylene glycol was added to the solution (precursor C) while stirring at room temperature for 30 minutes. Subsequently, the solution (precursor D) was diluted with n-propanol to 0.5 mol/L to form a transparent sol, and then aged for 24 h to form a transparent gel. The gel was then dried (120 °C for 12 h), calcined, and ground to obtain nanopowders. Various temperatures (540, 560, 580, 600, and 620 °C) were attempted to optimize the calcination temperature. After calcination, the powders were ground and then pressed into discs with a diameter of 11.5 mm and thickness of ~1.2 mm under a pressure of 6 MPa. PLZST ceramics were eventually obtained by sintering the discs at 1080 or 1100 °C for 2 h in air. Flow chart of the sol-gel process for obtaining the PLZST ceramics is illustrated in

Figure 1. For comparison, PLZST ceramics were also prepared by the traditional solid-state reaction method, following procedures reported in our previous work.²² Silver pastes (SA-5021, Wuhan Youle Optoelectronics Technology Co., Ltd.) were screen-printed onto both sides of the polished ceramics with a screen mesh of 250 lines per inch, and then fired at 550 °C for 10 min to form electrodes for the electrical measurements.

The phase structures of calcined nanopowders and sintered ceramics were characterized using x-ray diffraction (XRD; D8 Advanced, Bruker, Germany). The morphology observation of the nanopowders and element mapping tests of the ceramics were performed using a field-emission scanning electron microscope (FE-SEM; SIGMA 500, Zeiss, Germany) equipped with an energy dispersive spectrometer (EDS; XFlash 6130, Bruker, Germany). The particle size distribution of the powders was determined by nanoparticle size and potential analyzer (Zetasizer Nano ZS90, Malvern, UK). The surface microstructure of the ceramics was examined using scanning electron microscopy (SEM; JSM 6510LV, Jeol, Tokyo, Japan). The polarization versus electric field (*P-E*) hysteresis loops were measured with the ceramics in silicone oil using a ferroelectric testing system (PolyK Technologies, USA) combined with a high voltage amplifier (Trek 610E; Trek, Lockport, NY, USA) at 10 Hz. Based on the *P-E* hysteresis loops, energy-storage density and efficiency were calculated.

3. RESULTS AND DISCUSSION

Figure 2 shows XRD patterns of the PLZST powders prepared at various calcination temperatures. For the powders calcined at a low temperature of 540 °C, sharp diffraction peaks from the perovskite phase are observed along with a weak peak from the pyrochlore phase.³⁰ For perovskite oxides, the pyrochlore phase is commonly occurred at a low calcination temperature prior to eventual formation of the perovskite phase.³¹ Upon raising the calcination temperature to 580 °C, the peak of the pyrochlore phase is completely eliminated, and PLZST

powders with single-perovskite-phase are obtained. In order to give more insight into the phase structure of the powders, fine XRD pattern in the 2 range of 43°-45° is recorded as shown in the inset A. Two splitting peaks of (200) and (002) are observed clearly, which indicates a tetragonal AFE characteristic for the calcined powders. The insets B and C depict respectively the microscopic morphology and the particle size distribution of the powders. As seen, the average particle size of the powders is about 200nm. As the calcination temperature continues to increase up to 620 °C, Pb volatilization starts to occur, leading to reemergence of the pyrochlore phase. Therefore, the calcination temperature for the nanopowders used in preparing ceramics in this work is fixed at 580 °C.

Figure 3 displays XRD patterns of the PLZST ceramics sintered at 1080 and 1100 °C with the above-described nanopowders. Both ceramics exhibit a single-perovskite phase without any detectable secondary phase. Again the fine pattern shown in the inset confirms the tetragonal antiferroelectric character of the PLZST ceramics.

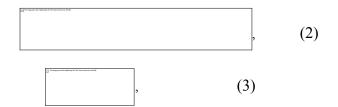
The surface microstructures of fresh PLZST ceramics sintered at 1080 °C and 1100 °C are shown in Figure 4. Ceramics with relatively uniform grains are obtained upon sintering at 1080 °C, but they are not dense and relatively large voids are observable on the ceramics surface. It indicates that the sintering temperature of 1080 °C is not high enough for driving the grain growth. Upon increasing the sintering temperature to 1100 °C, the grains become larger with an average size of about 1 µm, the voids disappear, and a dense ceramic is obtained.

To demonstrate advantages of the modified sol-gel method for making highly-active nanopowders, a comparison between the ceramics sintered with powders prepared by traditional solid state reaction method and the sol-gel-derived nanopowders is carried out in terms of phase structure, surface microstructure, and electrical properties, as presented in Fig. 5. From the XRD patterns in Fig. 5A, it is clearly seen that the modified sol-gel-derived ceramic possesses a single-perovskite phase structure, whereas appreciable segregation of Sn in the

form of SnO₂ appears in the ceramic prepared by the solid state reaction method. To further confirm the Sn segregation only occurs in the ceramic prepared by the solid state reaction method, we perform element-mapping tests of Sn for ceramics prepared by both methods, as shown in the insets of Figure 5A. While the Sn element is uniformly distributed in the modified sol-gel-derived ceramic, apparent Sn element segregation is observed in the ceramic prepared by the solid state reaction method. The causes for a higher solubility of Sn in the sol-gel-derived ceramic lattice than in the solid state reaction derived ceramic lattice may be two folds. Firstly, the wet-chemical based sol-gel synthesis offers a molecular-level intermixing of Sn with other elements. Secondly, the sol-gel-derived ceramic with smaller grains possesses far more abundant grain boundaries (cf. insets F and E of Fig. 5A), which allow effective release of strains caused by large-amount Sn incorporation into the PLZT lattice. Benefitting from the elimination of Sn segregation, as seen from the P-E hysteresis loops measured under the same electric field (Figure 5B), the sol-gel-derived ceramic (sintered at a low temperature of 1100 °C) exhibits far better energy storage capacity than the ceramic prepared by the solid state reaction method at a much higher sintering temperature (1230 °C). Thus, we only discuss the energy storage properties of PLZST ceramics prepared with the sol-gel method synthesized nanopowders in following sections.

Figure 6A illustrates room-temperature electric-field-dependent P-E loops of PLZST ceramics sintered at 1100 °C for 2 h. Typical double hysteresis loops reflects the AFE character of the ceramics. Upon increasing the electric field, the polarization gradually increases and reaches a maximum polarization of 34.2 μ C/cm² at 120 kV/cm. Figure 6B plots the energy-storage density W, recoverable energy-storage density W_{re}, and energy-storage efficiency \mathbb{F} , which are calculated using the following equations¹³:

(3) however the desired the first th	,	(1



where E is the applied electric field, and P, $P_{\rm r}$, and $P_{\rm max}$ are the spontaneous, remnant, and maximum polarization, respectively. As the applied electric field increases gradually, W and $W_{\rm re}$ tend to rise, whereas η declines. At the electric field of 120 kV/cm, the W and $W_{\rm re}$ show maximum values of 2.58 and 1.93 J/cm³, respectively, and the η reaches 75%.

For practical applications, the $W_{\rm re}$ and η maintaining high values over a wide temperature range is also very important. Thus, we further investigate the temperature dependence of the energy-storage performance of PLZST ceramics sintered at 1100 °C for 2 h at a fixed electric field of 120 kV/cm and a measuring frequency of 10 Hz, as presented in Figure 7A. The PLZST ceramics exhibit typical AFE double P-E hysteresis loops in a wide temperature range of 20-120 °C, and the P-E loops become slimmer with increasing temperature. The temperature dependences of P_{max} , E_{F} , E_{A} , and ΔE are summarized in Figure 7B. The P_{max} initially increases and then decreases with increasing temperature, reaching a maximum of 36.3 μC/cm² at 60 °C. The phase transition electric fields $E_{\rm F}$ and $E_{\rm A}$ continuously decrease as the temperature goes from 20 to 120 °C. This can be attributed to combined effects of the changing electric dipole interaction energy (W_{inter}) and the strain energy (W_{str}) during the AFE-FE phase transition. The $E_{\rm F}$ and $E_{\rm A}$ are respectively proportional to the sum $(W_{\rm inter} + W_{\rm str})$ and the difference $(W_{\rm inter} W_{\rm str}$) of electric-dipole interaction energy and strain energy. When the temperature rises, both W_{inter} and W_{str} decrease, and thus the E_{F} reduces. The reduction of E_{A} might be a result of higher decrease rate of the interaction energy between electric dipoles than the strain energy with rising temperature. 11 The W, $W_{\rm re}$ and η of the PLZST ceramics are shown in Figure 7C as a function of the temperature. Clearly, the W and W_{re} initially increase with rising temperature and then decrease, showing an inflection point at 60 °C, which is consistent with the variation in P_{max} . This result indicates that, in the temperature range of 20-120 °C, the W and W_{re} are mainly influenced by the P_{max} . At 60 °C, both W and W_{re} reach their maximum values of 2.78 and 2.24 J/cm³, respectively, and η reaches 81%. Besides, the W_{re} varies only slightly, keeping larger than 1.9 J/cm³ in the temperature range of 20-120 °C, which indicates that the modified sol-gel-derived PLZST ceramic is a promising candidate for making pulsed power capacitors operable over a broad temperature range.

4. CONCLUSION

In summary, $Pb_{0.97}La_{0.02}(Zr_{0.50}Sn_{0.45}Ti_{0.05})O_3$ nanopowders have been synthesized by a modified sol-gel method using a low-cost dibutyltin oxide instead of expensive tin acetate as tin precursor, and the obtained nanopowders show a single-perovskite structure and average particle diameter of 200 nm at a calcined temperature of 580 °C. PLZST AFE ceramics sintered with these nanopowders at relatively low temperature of 1100 °C show a pure perovskite phase and compact microstructure. The ceramics present a maximum room-temperature recoverable energy-storage density of 1.93 J/cm³ at electric field of 120 kV/cm and the energy density remains larger than 1.9 J/cm³ between 20 °C and 120 °C. At 60 °C, the ceramics exhibit the best energy-storage properties ($W_{re} = 2.24 \text{ J/cm}^3$, $\eta = 81\%$) due to the achievement of maximum P_{max} . The high energy-storage density and good stability in a wide temperature range suggest that $Pb_{0.97}La_{0.02}(Zr_{0.50}Sn_{0.45}Ti_{0.05})O_3$ AFE ceramics prepared by the sol-gel method with a low-cost tin precursor hold great application potential in pulse power capacitors.

ACKNOWLEDGMENTS

The authors gratefully acknowledge the National Natural Science Foundation of China (Grant Nos. 61274010, 51572073, 51602093, 11774082), the Natural Science Foundation of Hubei Province (Grant Nos. 2015CFA119, 2016AAA031, 2018CFB700), State Key

Laboratory of Advanced Technology for Materials Synthesis and Processing (Wuhan University of Technology; Grant No. 2018-KF-16).

REFERENCES

- 1. Dang ZM, Yuan JK, Yao SH, Liao RJ. Flexible nanodielectric materials with high permittivity for power energy storage. Adv Mater. 2013;25:6334.
- 2. Yao K, Chen ST, Rahimabady M, Mirshekarloo MS, Yu SH, et al. Nonlinear dielectric thin films for high-power electric storage with energy density comparable with electrochemical supercapacitors. IEEE Trans Ultrason Ferroelectr Freq Control. 2011;58:1968-1974.
- 3. Peng BL, Zhang Q, Li X, Sun TY, Fan HQ, Ke SM, Ye M, et al. Giant electric energy density in epitaxial lead-free thin films with coexistence of ferroelectrics and antiferroelectrics. Adv Electron Mater. 2015;1:1500052.
- 4. Ahn CW, Amarsanaa G, Won SS, Chae SA, Lee DS, Kim IW. Antiferroelectric thin-film capacitors with high energy-storage densities, low energy losses, and fast discharge times. ACS Appl Mater Interfaces. 2015;7:26381-26386.
- 5. Hao XH. A review on the dielectric materials for high energy-storage application. J Adv Dielectrics. 2013;3:1330001.
- 6. Zhang X, Shen Y, Zhang QH, Gu L, Hu YH, et al. Ultrahigh energy density of polymer nanocomposites containing BaTiO₃@TiO₂ nanofibers by atomic-scale interface engineering. Adv Mater. 2015;27:819-824.
- 7. Peng BL, Zhang Q, Li X, Sun TY, Fan HQ, et al. Large energy storage density and high thermal stability in a highly textured (111)-oriented Pb_{0.8}Ba_{0.2}ZrO₃ relaxor thin film with the coexistence of antiferroelectric and ferroelectric phases. ACS Appl Mater Interfaces. 2015;7:13512.
- 8. Liu GC, Fan HQ, Dong GZ, Shi J, Chang Q. Enhanced energy storage and dielectric properties of Bi_{0.487}Na_{0.427}K_{0.06}Ba_{0.026}TiO_{3-x}CeO₂ anti-ferroelectric ceramics. J Alloy Comp. 2016;664:632-638.
- 9. Zhang L, Jiang SL, Zeng YK, Fu M, Han K, Li Q, Wang Q, Zhang GZ. Y doping and grain

- size co-effects on the electrical energy storage performance of $(Pb_{0.87}Ba_{0.1}La_{0.02})(Zr_{0.65}Sn_{0.3}Ti_{0.05})O_3 \quad anti-ferroelectric \quad ceramics. \quad Ceram \quad Int. \\ 2014;40:5455-5460.$
- 10. Zhang QF, Tong HF, Chen J, Lu YM, Yang TQ, Yao X, He YB. High recoverable energy density over a wide temperature range in Sr modified (Pb,La) (Zr,Sn,Ti)O₃ antiferroelectric ceramics with an orthorhombic phase. Appl Phys Lett. 2016;109: 262901.
- Zhang HL, Chen XF, Cao F, Wang GS, Dong XL. Charge-discharge properties of an antiferroelectric ceramics capacitor under different electric fields. J Am Ceram Soc. 2010;93:4015-4017.
- 12. Chu BJ, Zhou X, Ren KL, Neese B, Lin MR, Wang Q, Bauer F, Zhang QM. A dielectric polymer with high electric energy density and fast discharge speed. Science. 2006;313:334-336.
- 13. Liu Z, Chen XF, Peng W, Xu CH, Dong XL, Cao F, Wang GS, Temperature-dependent stability of energy storage properties of Pb_{0.97}La_{0.02}(Zr_{0.58}Sn_{0.335}Ti_{0.085})O₃ antiferroelectric ceramics for pulse power capacitors. Appl Phys Lett. 2015;106:262901.
- 14. Zhang QF, Yang TQ, Zhang YY, Yao X. Phase transition and electric field induced strain properties in Sm modified lead zirconate stannate titanate based antiferroelectric ceramics. J Appl Phys. 2013;113:244103.
- 15. Zhang QF, Chen J, Lu YM, Yang TQ, Yao X, He YB. (Pb,Sm)(Zr,Sn,Ti)O₃ Multifunctional ceramics with large electric-field-induced strain and high-energy storage density. J Am Ceram Soc. 2016;99:3853-3856.
- Liu Z, Dong XL, Liu Y, Cao F, Wang GS. Electric field tunable thermal stability of energy storage properties of PLZST antiferroelectric ceramics. J Am Ceram Soc. 2017;100:2382-2386.
- 17. Xu R, Tian JJ, Zhu QS, Feng YJ, Wei XY, Xu Z. Effect of temperature-driven phase

- transition on energy-storage and -release properties of $Pb_{0.97}La_{0.02}[Zr_{0.55}Sn_{0.30}Ti_{0.15}]O_3$ ceramics. J Appl Phys. 2017;122:024104.
- 18. Xu R, Tian JJ, Zhu QS, et al. Effects of phase transition on discharge properties of PLZST antiferroelectric ceramics. J Am Ceram Soc. 2017;100:3618-3625.
- 19. Liu Z, Bai Y, Chen XF, Dong XL, Nie HC, Cao F, Wang GS. Linear composition-dependent phase transition behavior and energy storage performance of tetragonal PLZST antiferroelectric ceramics. J Alloy Comp. 2017;691:721-725.
- 20. Xu R, Zhu QS, Tian JJ, Feng YJ, Xu Z. Effect of Ba-dopant on dielectric and energy storage properties of PLZST antiferroelectric ceramics. Ceram Int. 2017;43:2481-2485.
- 21. Zhang QF, Dan Y, Chen J, Lu YM, Yang TQ, Yao X, He YB. Effects of composition and temperature on energy storage properties of (Pb,La)(Zr,Sn,Ti)O₃ antiferroelectric ceramics. Ceram Int. 2017;43:11428-11432.
- 22. Chen M, Yao X, Zhang LY. Preparation of (Pb,La)(Zr,Sn,Ti)O₃ antiferroelectric ceramics using colloidal processing and the field-induced strain properties. J Eur Ceram Soc. 2001;21:1159-1164.
- 23. Xue LH, Li Q, Zhang YL, Liu R, Zhen XH. Synthesis, sintering and characterization of PLZST perovskite prepared by a lactate precursor route. J Eur Ceram Soc. 2006;26:323-329.
- 24. Wang L, Li Q, Xue LH, Liang XM. Effect of Ti⁴⁺:Sn⁴⁺ ratio on the phase transition and electric properties of PLZST antiferroelectric ceramics. J Mater Sci. 2007;42:7397-7401.
- 25. Traianidis M, Courtois C, Leriche A. Mechanism of PZT crystallisation under hydrothermal conditions development of a new synthesis route. J Eur Ceram Soc. 2000;20:2713-2720.
- 26. Linardos S, Zhang Q, Alcock JR. Preparation of sub-micron PZT particles with the sol-gel technique. J Eur Ceram Soc. 2006;26:117-123.

- 27. Chen M, Yao X, Zhang L. Grain size dependence of dielectric and field-induced strain properties of chemical prepared (Pb,La)(Zr,Sn,Ti)O₃ antiferroelectric ceramics. Ceram Int. 2002; 28:201-207.
- 28. Zhai JW, Chen H. Crystallization kinetics and dielectric properties in sol-gel derived (Pb, La) (Zr, Sn Ti)O₃ ceramics. J Appl Phys. 2003; 94: 589 593.
- 29. Lee JH, Chiang YM. Pressure-induced pyrochlore-perovskite phase transformation in PLZST ceramics. J Electroceram. 2001; 6: 7-12.
- 30. Wu AY, Vilarinho PM, Salvado IMM, Baptista JL. Sol-Gel Preparation of Lead Zirconate Titanate Powders and Ceramics: Effect of Alkoxide Stabilizers and Lead Precursors. J Am Ceram Soc. 2000; 83:1379-85.

Figure Captions:

FIGURE 1: The flow chart of the sol-gel processing for PLZST ceramics.

FIGURE 2: XRD patterns of PLZST powders calcined at various temperatures. The insets (A), (B) and (C) show respectively the fine XRD pattern in the 2θ range of 43° - 45° , the FESEM image and the particle size distribution of PLZST powders calcined at 580° C.

FIGURE 3: XRD patterns of PLZST ceramics sintered at 1080 and 1100 °C. The inset shows the fine XRD pattern in the 2θ range of 43° - 45° .

FIGURE 4: Surface SEM images of PLZST ceramics sintered at (A) 1080 °C and (B) 1100 °C.

FIGURE 5: (A) XRD patterns and (B) *P-E* loops measured under the same electric field of PLZST ceramics derived respectively from the solid state reaction method (sintering temperature of 1230 °C) and the modified sol-gel method (sintering temperature of 1100 °C). The insets show the EDS mapping of Sn (C, D) and surface morphology (E, F) for corresponding ceramics.

FIGURE 6: Electric-field-dependent (A) P-E loops, and (B) energy densities (storage energy density W and recoverable energy density W_{re}) and energy efficiency (η) measured at room temperature for PLZST ceramics sintered at 1100 °C.

FIGURE 7: (A) *P-E* loops at different temperatures, and effects of temperature on (B) ferroelectric and (C) energy storage properties of PLZST ceramics sintered at 1100 °C.

Cranfield University

CERES https://dspace.lib.cranfield.ac.uk

School of Aerospace, Transport and Manufacturing (SATM)

Staff publications (SATM)

2018-08-31

High energy density of PLZST antiferroelectric ceramics prepared by sol-gel method with low-cost dibutyltin oxide

Dan, Yu

Wiley

Yu Dan, Haojie Xu, Yangyang Zhang, et al., High energy density of PLZST antiferroelectric ceramics prepared by sol-gel method with low-cost dibutyltin oxide. Journal of the American Ceramic Society, Volume 102, Issue 4, 2019, pp. 1776-1783

https://doi.org/10.1111/jace.16041

Downloaded from Cranfield Library Services E-Repository